Inorg. Chem. **2005**, *44*, 3194–3202

Structural and Magnetic Diversity in Tetraalkylammonium Salts of Anionic $M[N(CN)_2]_3^-$ (M = Mn and Ni) Three-Dimensional Coordination Polymers

John A. Schlueter,*,† Jamie L. Manson,‡ and Urs Geiser†

Materials Science Division, Argonne National Laboratory, Argonne, Illinois 60439-4831, and Department of Chemistry and Biochemistry, Eastern Washington University, Cheney, Washington 99004

Received November 3, 2004

Tetraalkylammonium cations, $(NR_4)^+$ (R = C_3H_7, C_4H_9, and C_5H_{11}), have been used as templates to form a new family of $[M(dca)_3]^-$ [M = Mn and Ni; dca = dicyanamide or $N(CN)_2^-$] salts. The tetrapropylammonium (TPrA) salts possess a perovskite-type anion structure. (TPrA)[Mn(dca)$_3$] (**1**) crystallizes in the tetragonal space group $P\bar{4}2_1c$, with a = 16.2945(8) Å, c = 17.4321(8) Å, and V = 4628.4(6) Å^3 at T = 298 K. At room temperature, (TPrA)[Ni(dca)$_3$] (**2**) crystallizes in the orthorhombic space group *Pnna*, with a = 17.171(2) Å, b = 22.992(2) Å, c = 22.750(2) Å, and V = 8981(2) Å^3, but undergoes a first-order phase transition within the temperature range 150–220 K to the tetragonal space group $P\bar{4}2_1c$, with a = 16.0985(7) Å, c = 17.0287(8) Å, and V = 4413.2(5) Å^3 at T = 160 K. At 110 K, **2** returns to the *Pnna* space group with a = 17.116(2) Å, b = 22.800(3) Å, c = 22.641(3) Å, and V = 8835(3) Å^3. The tetrabutylammonium (TBA) salts possess a triple rutile structure. (TBA)[Mn(dca)$_3$] (**3**) crystallizes in the orthorhombic space group $P2_12_12$, with a = 16.0107(6) Å, b = 16.0114(6), c = 21.5577(8) Å, and V = 5526.4(5) Å^3. (TBA)[Ni(dca)$_3$] (**4**) also crystallizes in the orthorhombic space group $P2_12_12$, with a = 15.6842(5) Å, b = 15.6841(6) Å, c = 21.1551(8) Å, and V = 5204.0(5) Å^3. The tetrapentylammonium (TPnA) salts crystallize with a $LiSbO_3$ structure type, space group *Pnna*. Lattice parameters for (TPnA)[Mn(dca)$_3$] (**5**) are a = 13.2236(6) Å, b = 11.6300(6) Å, c = 20.3176(9) Å, and V = 3124.6(4) Å^3, and for (TPnA)[Ni(dca)$_3$] (**6**), a = 12.9380(4) Å, b = 11.6233(4) Å, c = 19.8038(7) Å, and V = 2978.1(2) Å^3. Long-range antiferromagnetic ordering has been observed in the manganese salts below 2.1 K, as indicated by alternating current susceptibility measurements. Magnetic susceptibility data for the nickel salts do not show evidence for long-range magnetic ordering but can be described using an S = 1 zero-field splitting model with the exchange Hamiltonian $\mathcal{H} = -J\sum S_iS_{i+1} + D\sum(S_i^z)^2 + g\mu_\beta B\sum S_i$, giving $|D|/k_B$ values that range between 1.98(1) K and 3.20(2) K.

Introduction

The coordination polymers that are formed when divalent first-row transition metals are linked with the generally bidentate (monodentate and tridentate coordination is also possible) dicyanamide [dicyanamide is $N(CN)_2^-$, hereafter abbreviated as dca] anion are of current research interest because of their structural diversity and potential for magnetic ordering.[1] The majority of the transition metal dca complexes possess low-dimensional (chain or layer) structural motifs, whereas three-dimensional coordination solids are less frequently observed.

The prime examples of previously reported three-dimensional dca networks are the neutral, binary systems, $M(dca)_2$ (M = V, Cr, Mn, Fe, Co, Ni, and Cu), which form rutile-like structures that exhibit ferromagnetic, antiferromagnetic, or paramagnetic ground states. For example, the $Ni(dca)_2$ complex has a ferromagnetic ground state, with a Curie temperature of 21 K,[2,3] $Mn(dca)_2$ is an antiferromagnet with a Néel temperature of 16 K,[4] and $Cu(dca)_2$ is paramag-

* Author to whom correspondence should be addressed. E-mail: JASchlueter@anl.gov.
† Argonne National Laboratory.
‡ Eastern Washington University.

(1) Batten, S. R.; Murray, K. S. *Coord. Chem. Rev.* **2003**, *246*, 103.
(2) Manson, J. L.; Kmety, C. R.; Huang, Q. Z.; Lynn, J. W.; Bendele, G. M.; Pagola, S.; Stephens, P. W.; Liable-Sands, L. M.; Rheingold, A. L.; Epstein, A. J.; Miller, J. S. *Chem. Mater.* **1998**, *10*, 2552.
(3) Kurmoo, M.; Kepert, C. *New J. Chem.* **1998**, *12*, 1515.

10.1021/ic0484598 CCC: $30.25 © 2005 American Chemical Society
Published on Web 04/02/2005

netic down to 2 K.[5] In these salts, additional coordination to the central amide nitrogen is observed.

Although anionic $[M(dca)_3]^-$ (M = Co and Ni) complexes were first reported more than 30 years ago,[6,7] their structural and magnetic properties have not been characterized until more recently. A novel anionic, one-dimensional, ladder-type structure was observed for the solvated $(Ph_4As)_2[M_2(dca)_6(H_2O)]\cdot H_2O\cdot xCH_3OH$ (M = Co and Ni) salts in which the sides of the ladder are composed of doubly bridged dca ligands, the rungs are composed of a disordered dca bridge, and the remaining octahedral sites are composed of disordered terminal dca and water ligands.[8] Isomorphous $(Ph_4E)[Mn(dca)_3]$ (E = P, As) and $(Ph_4P)[Co(dca)_3]$ structures are characterized by two-dimensional anionic sheets composed of metal atoms that are bridged by two dca anions in one direction and a single, disordered dca bridge in the other.[9,10] In the closely related $(Ph_4As)[M(dca)_3]$ (M = Co and Ni) structures, the single dca bridge is ordered, resulting in a doubling of the b axis.[8] The addition of 1 equiv of $(Ph_4P)(dca)$ to $(Ph_4P)[Co(dca)_3]$ results in the formation of $(Ph_4P)_2[Co(dca)_4]$, which possesses a doubly bridged chain structure with two terminal dca ligands per cobalt.[10,11] Hexagonal anionic sheets, in which the manganese atoms are bi-bridged by dca anions, are found in the $[M(bipy)_3][Mn(dca)_3]_2$ (M = Fe and Ni; bipy = 2,2′-bipyridine) salts.[12]

Cation templating has been shown to play an important role in determining the anionic structure. By replacing one phenyl group with a methyl group, adjacent two-dimensional $[Mn(dca)_3]^-$ sheets of $(Ph_4P)[Mn(dca)_3]$ are condensed into a three-dimensional network, leading to the first example of a three-dimensional anionic $[M(dca)_3]^-$ lattice type in the $(MePh_3P)[Mn(dca)_3]$ salt.[9] In this salt, two-dimensional sheets are formed by both single and double dca bridges between manganese centers. These two-dimensional sheets are linked in the third dimension by single dca bridges, forming a distorted triple rutile structure.

The construction of a simple cubelike $[M(dca)_3]^-$ structure with single dca bridges in all three directions has been of interest in order to gain a more complete understanding of magnetic interaction pathways, as well as for the development of porous networks for the storage of volatile molecules or catalysis applications. Such structures could be prone to interpenetration, which is commonly seen in three-dimensional network solids such as $Mn(dca)_2(pyz)$.[13,14] Interpenetration can be avoided if molecules of the appropriate size and shape can be cocrystallized to fill the voids. Such a strategy has recently been employed to form anionic NaCl-type frameworks of $[Mn(HCOO)_3]^-$ that have been templated by alkylammonium cations.[15] Anionic $[Mn(dca)_3]^-$ lattices are promising candidates for the formation of three-dimensional, noninterpenetrating lattices, if a charge compensating cation can adequately fill the structural void. The first examples of such structures, $A[M(dca)_3]$ (A = benzyltributylammonium, M = Mn, Co; A = benzyltriethylammonium, M = Mn, Fe), did not show long-range magnetic ordering above 2 K.[13] More recently, we have found that a similar three-dimensional anionic cube-type structure, which exhibits long-range antiferromagnetic ordering below 2.5 K, forms when SPh_3^+ is used as the templating cation.[16] In the present paper, we report the use of tetraalkylammonium (hereafter abbreviated as TAA) cations as templates for the formation of three-dimensional, homoleptic $[M(dca)_3]^-$ structures. TAA^+ cations were selected because they offer the promise of a closely related series with finely tunable sizes, thus, leading to a better understanding of the templating effects.

Experimental Section

Materials. (TBA)Br (Aldrich; TBA = tetrabutylammonium), Na(dca) (Lonza), (TPrA)Br (Aldrich; TPrA = tetrapropylammonium), (TPnA)Br (Aldrich; TPnA = tetrapentylammonium), $Mn(NO_3)_2\cdot xH_2O$ (Aldrich), $MnBr_2$ (Alfa), $Ni(NO_3)_2\cdot 6H_2O$ (Aldrich), and ethanol (Aaper, 200 proof) were used as received.

Synthesis of (TAA)[M(dca)$_3$] (1−6). (TAA)Br (2 mmol) was dissolved in 10 mL of ethanol and combined with a solution of Na(dca) (6 mmol) in 10 mL of water. This mixture was layered on top of a solution of $M(NO_3)_2\cdot xH_2O$ (2 mmol) in 10 mL of water. In the case of $(TPnA)[Mn(dca)_3]$, $MnBr_2$ was used as the metal source, although similar results would be expected with the use of $Mn(NO_3)_2\cdot xH_2O$. After about 2 weeks, colorless blocky crystals were collected by filtration.

(TPrA)[Mn(dca)$_3$] (1). Mp: 255−260 °C dec. Anal. Calcd (%) for $C_{18}H_{28}N_{10}Mn$: C, 49.20; H, 6.42; N, 31.88. Found: C, 48.59; H, 6.37; N, 31.38. IR (KBr/cm^{-1}) ν_{CN}: 2291s, 2238m, 2175vs.

(TPrA)[Ni(dca)$_3$] (2). Mp: 265−270 °C dec. Anal. Calcd (%) for $C_{18}H_{28}N_{10}Ni$: C, 48.62; H, 6.41; N, 31.41. Found: C, 48.62; H, 6.41; N, 31.41. IR (KBr/cm^{-1}) ν_{CN}: 2291s, 2254m, 2190vs.

(TBA)[Mn(dca)$_3$] (3). Mp: 181−184 °C. Anal. Calcd (%) for $C_{22}H_{36}N_{10}Mn$: C, 53.32; H, 7.32; N, 28.27. Found: C, 53.23; H, 7.41; N, 27.98. IR (KBr/cm^{-1}) ν_{CN}: 2287s, 2234m, 2170vs.

(TBA)[Ni(dca)$_3$] (4). Mp: 194−196 °C. Anal. Calcd (%) for $C_{22}H_{36}N_{10}Ni$: C, 52.92; H, 7.27; N, 28.05. Found: C, 52.89; H, 7.27; N, 27.93. IR (KBr/cm^{-1}) ν_{CN}: 2289s, 2242m, 2180vs.

(TPnA)[Mn(dca)$_3$] (5). Mp: 152−154 °C. Anal. Calcd (%) for $C_{26}H_{44}N_{10}Mn$: C, 56.61; H, 8.04; N, 25.39. Found: C, 56.72; H, 7.96; N, 25.33. IR (KBr/cm^{-1}) ν_{CN}: 2292s, 2233m, 2166vs.

(TPnA)[Ni(dca)$_3$] (6). Mp: 162−164 °C. Anal. Calcd (%) for $C_{26}H_{44}N_{10}Ni$: C, 56.23; H, 7.99; N, 25.22. Found: C, 55.14; H, 8.00; N, 24.81. IR (KBr/cm^{-1}) ν_{CN}: 2292s, 2242m, 2181vs.

(4) Batten, S. R.; Jensen, P.; Kepert, C. J.; Kurmoo, M.; Moubaraki, B.; Murray, C. B.; Price, D. J. *J. Chem. Soc., Dalton Trans.* **1999**, 2987.
(5) Kurmoo, M.; Kepert, C. J. *Mol. Cryst. Liq. Cryst. Sci. Technol., Sect. A* **1999**, *334*, 693.
(6) Köhler, V. H.; Seifert, B. *Z. Anorg. Allg. Chem.* **1966**, *344*, 63.
(7) Köhler, V. H.; Hartung, H.; Golub, A. M. *Z. Anorg. Allg. Chem.* **1974**, *403*, 41.
(8) van der Werff, P.; Batten, S. R.; Jensen, P.; Moubaraki, B.; Murray, K. S.; Tan, E. H. K. *Polyhedron* **2001**, *20*, 1129.
(9) van der Werff, P.; Batten, S. R.; Jensen, P.; Moubaraki, B.; Murray, K. S. *Inorg. Chem.* **2001**, *40*, 1718.
(10) Raebiger, J. W.; Manson, J. L.; Sommer, R. D.; Geiser, U.; Rheingold, A. L.; Miller, J. S. *Inorg. Chem.* **2001**, *40*, 2578.
(11) Jager, L.; Wagner, C.; Korabik, M.; Zygmunt, A.; Mrozinski, J. *J. Mol. Struct.* **2001**, *570*, 159.
(12) Batten, S. R.; Jensen, P.; Moubaraki, B.; Murray, K. S. *J. Chem. Soc., Chem. Commun.* **2000**, 2331.
(13) Tong, M. L.; Ru, J.; Wu, Y. M.; Chen, X. M.; Chang, H. C.; Mochizuki, K.; Kitagawa, S. *New J. Chem.* **2003**, *27*.
(14) Manson, J. L.; Incarvito, C. D.; Rheingold, A. L.; Miller, J. S. *J. Chem. Soc., Dalton Trans.* **1998**, 3705.
(15) Wang, Z.; Zhang, B.; Otsuka, T.; Inoue, K.; Kobayashi, H.; Kurmoo, M. *J. Chem. Soc., Dalton Trans.* **2004**, 2209.
(16) Schlueter, J. A.; Manson, J. L.; Hyzer, K. A.; Geiser, U. *Inorg. Chem.* **2004**, *43*, 4100.

Table 1. X-ray Crystallographic Data for Compounds **1**−**6**. For All Compounds, $\alpha = \beta = \gamma = 90°$ and $\lambda = 0.71\,073$ Å.

	1	**1**	**2**	**2**	**2**
formula	$C_{18}H_{28}N_{10}Mn$	$C_{18}H_{28}N_{10}Mn$	$C_{18}H_{28}N_{10}Ni$	$C_{18}H_{28}N_{10}Ni$	$C_{18}H_{28}N_{10}Ni$
a (Å)	16.2945(8)	16.1461(6)	17.171(2)	16.0985(7)	17.116(2)
b (Å)	16.2945(8)	16.1461(6)	22.992(2)	16.0985(7)	22.800(3)
c (Å)	17.4321(8)	17.4126(13)	22.750(2)	17.0287(8)	22.641(3)
V (Å^3)	4628.4(6)	4539.4(9)	8981(2)	4413.2(5)	8835(3)
Z	8	8	16	8	16
fw	439.44	439.44	443.21	443.21	443.21
space group	$P\bar{4}2_1c$ (#114)	$P\bar{4}2_1c$ (#114)	*Pnna* (#52)	$P\bar{4}2_1c$ (#114)	*Pnna* (#52)
T (K)	298	180	298	160	110
ρ_{calc} (g cm^{-3})	1.261	1.286	1.311	1.334	1.333
μ (cm^{-1})	0.59	0.61	0.89	0.90	0.90
$R(F_0)^a$	0.0425	0.0519	0.0582	0.0658	0.0382
$R_w(F_0)^b$	0.1194	0.1126	0.1512	0.1675	0.0931

	3	**4**	**5**	**6**
formula	$C_{22}H_{36}N_{10}Mn$	$C_{22}H_{36}N_{10}Ni$	$C_{26}H_{44}N_{10}Mn$	$C_{26}H_{44}N_{10}Ni$
a (Å)	16.0107(6)	15.6842(5)	13.2236(6)	12.9380(4)
b (Å)	16.0114(6)	15.6841(6)	11.6300(6)	11.6233(4)
c (Å)	21.5577(8)	21.1551(8)	20.3176(9)	19.8038(7)
V (Å^3)	5526.4(5)	5204.0(5)	3124.6(4)	2978.1(2)
Z	8	8	4	4
fw	495.53	499.32	551.65	555.42
space group	$P2_12_12$ (#18)	$P2_12_12$ (#18)	*Pnna* (#52)	*Pnna* (#52)
T (K)	298	298	298	298
ρ_{calc} (g cm^{-3})	1.191	1.275	1.173	1.239
μ (cm^{-1})	0.51	0.78	0.45	0.68
$R(F_0)^a$	0.0376	0.0389	0.0609	0.0452
$R_w(F_0)^b$	0.1071	0.1025	0.1930	0.1304

[a] $R(F_0) = \sum||F_o| - |F_c||/\sum|F_0|$ ($I > 2\sigma$). [b] $R_w(F_0^2) = [\sum w(|F_0^2| - |F_c^2|)^2/\sum wF_0^2]^{1/2}$ (all data).

X-ray Crystallography. The crystal structure of compounds **1**−**6** were determined by X-ray diffraction using a Siemens SMART single-crystal diffractometer equipped with a charge coupled device-based area detector and a sealed-tube Mo Kα source. The detector frames were integrated by the use of the SAINT program[17] and the intensities corrected for absorption by Gaussian integration on the basis of the measured crystal shape using the XPREP program of SHELXTL.[17] Other systematic variations were corrected by the analysis of replicate reflections using the SADABS program.[18] Low-temperature data were collected with a regulated boil-off stream from liquid nitrogen. The structure solutions were carried out using direct methods. Full-matrix least-squares refinement on F^2 (including all data) was performed using the SHELXTL program.[19] These crystal structures are complicated by disorder, both in the dca ligands[20] and in the TAA cations. In addition, several of these structures were solved on the basis of diffraction data from pseudomerohedrally twinned crystals. A summary of the crystallographic data is given in Table 1, the atomic numbering schemes are illustrated in the Supporting Information, Figures S1−S9, and further details of each structure are available in the CIF files also deposited as electronic supporting information.

Magnetic Measurements. The direct current (dc) magnetizations of the nickel compounds (**2**, **4**, and **6**) were measured between 5 and 300 K using a Quantum Design (San Diego, CA) MPMS-5 SQUID magnetometer. A collection of crystals of each compound was tightly packed in gelatin capsules, mounted in a plastic straw, and affixed to the end of the sample rod. Samples weighing 75−105 mg were cooled in a zero field to the lowest temperature of 5 K. The magnetization was measured as a function of the field up to 5 T. The dc field was then charged to 1 kOe, and the magnetization data were recorded upon warming. All magnetic data were corrected for core diamagnetism using Pascal's constants.

The dc magnetizations of the manganese compounds (**1**, **3**, and **5**) were measured between 2 and 300 K using a Quantum Design (San Diego, CA) PPMS-9 magnetometer. Multiple crystals of each compound were mounted as above. Samples weighing 48−112 mg were cooled in a zero field to the lowest temperature of 2 K. The magnetization was measured as a function of the field up to 9 T. The dc field was then charged to 1 kOe, and the magnetization data were recorded upon warming. All magnetic data were corrected for core diamagnetism using Pascal's constants.

Alternating current (ac) susceptibility measurements were performed on a Lake Shore Cryotronics 7000 series susceptometer equipped with a low-temperature helium subpot option (allowing measurements to be achieved at temperatures as low as 1.5 K) and operated at a frequency of 125 Hz and an amplitude of 1 or 2 Oe. Polycrystalline samples of **2**, **4**, **5**, and **6** were loaded into a Delrin sample cup, which was screwed onto the end of a Delrin isolation rod. Blocklike single crystals of **1** (19.064 mg) and **3** (20.478 mg) were supported on the end of the isolation rod with a minimum amount of Apiezon N grease. The samples were cooled from room temperature to 4.5 K over a period of 15 min, then further cooled to 1.5 K over a period of 45 min. The real (in-phase, χ') and imaginary (out-of-phase, χ'') components of the volume ac susceptibility were recorded at temperature intervals of 0.05 K for bulk samples and 0.025 K for single-crystal specimens. Magnetic field sweeps were run at 1.8 K from 0 to 45 kOe in steps as small as 100 Oe through the magnetic transition regions.

Infrared Spectroscopy. Samples were ground into KBr (Aldrich) and pressed into pellets. Infrared spectra were collected on a Nicolet 510P Fourier transform infrared spectrometer operated with OMNIC

(17) *SAINT*, version 6.28a; Bruker AXS, Inc.: Madison, WI, 1996.
(18) Sheldrick, G. M. *SADABS*, version 2.03a; Bruker AXS, Inc.: Madison, WI, 2001.
(19) Sheldrick, G. M. *SHELXTL*, version 6.12; Bruker AXS, Inc.: Madison, WI, 2001.
(20) The dca disorder is a libration around the axis formed by the nitrile nitrogen atoms. It does not affect the topology of the $M(dca)_3^-$ network.

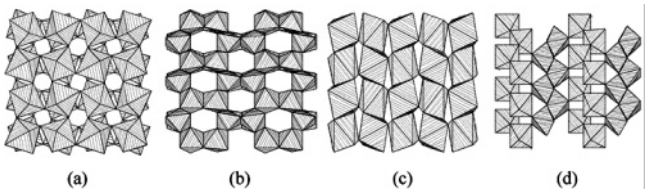

Figure 1. Polyhedral representation of various structural motifs observed in the three-dimensional $[M(dca)_3]^-$ anions. Polyhedrons are drawn with the corners defined as the amide nitrogen atoms of the dca anions. (a) 2 × 2 × 2 perovskite structure. (b) Triple rutile structure. (c) $LiSbO_3$-type structure, viewed along the *c* axis. (d) $LiSbO_3$-type structure, viewed approximately along the [110] direction.

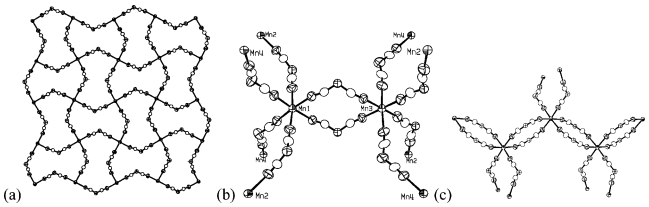

Figure 2. (a) Projection of the anion layer of the structure of **1** in the *ab* plane. These layers are linked in the third dimension by $\mu_{1,5}$-dca$^-$ anions, completing the octahedral coordination about the manganese center and forming a pseudocubic anion framework that surrounds the TPrA$^+$ cation. (b) The doubly bridged dimer units in **3** are further linked into a three-dimensional network through single $\mu_{1,5}$-dca$^-$ bridges. (c) The cis bi-bridged zigzag chains in (TPnA)[Ni(dca)$_3$] are singly bridged together to form a three-dimensional $LiSbO_3$-type network. For all of the figures, only one component of the disordered dca groups is shown for clarity. Metal atoms are depicted with shaded octants, nitrogen atoms are depicted with open octants, and carbon atoms are depicted as open ellipsoids.

version 4.1a software. Spectra were averaged over 32 scans with a 2 cm^{-1} resolution.

Elemental Analysis. Carbon, hydrogen, and nitrogen elemental analyses were performed by Midwest Microlab (Indianapolis, IN).

Results

Crystal Structures. Perovskite Structures (1 and 2). As shown in Figure 1a, the three-dimensional anionic lattice in **1** is characterized as a 2 × 2 × 2 perovskite superlattice. This structure possesses two-dimensional sheets of Mn(dca)$_2$ parallel to the *ab* plane, as illustrated in Figure 2a. These sheets are joined in the third dimension by $\mu_{1,5}$-dca$^-$ anions, which complete the octahedral coordination about the manganese center, thus, forming a cubic anion framework that surrounds the TPrA$^+$ cation. Thus, all manganese atoms are singly bridged by $\mu_{1,5}$-dca$^-$ in all six directions to afford the three-dimensional framework. Compared to the hypothetical perovskite prototype, the superlattice is formed by an antiferro-distortively coupled rotation of the coordination octahedra around the *c* axis.

Compound **1** crystallizes in the $P\bar{4}2_1c$ space group. The Mn···Mn separations within the *ab* plane are 8.2274(2) and 8.2561(2) Å, whereas parallel to the *c* axis, it is slightly longer at 8.7522(4) Å. These distances decrease to 8.1785(3), 8.2174(3), and 8.7512 Å at 180 K. There is a considerable disorder in the dca amide-N positions at room temperature. The amide nitrogen atom (N11) of the dca anion that bridges the Mn centers along the *c* axis and the carbon atoms bonded to it were modeled to occupy four positions with occupancies of 33(1), 32(1), 16(1), and 19(1)% at room temperature, with similar values at 180 K using suitable geometric restraints. The amide nitrogen N12 and the carbon atoms bonded to it were modeled with three sites with occupancies of 46(1), 28(1), and 26(1)%, again, with similar values at 180 K. The manganese atom lies on a general position with the octahedral coordination sphere consisting of the nitrile nitrogen atoms of six dca anions. At room temperature, these Mn−N distances within the *ab* plane range from 2.210(2) to 2.243(2) Å, whereas along the *c* axis, the lengths are 2.200(2) and 2.219(2) Å. The C−N−Mn bond angles range from 153(1) to 172.6(3)°. Three crystallographically unique TPrA$^+$ cations are present, two of which lie on $\bar{4}$ sites, while the third lies on a 2-fold axis along *z*. Two of the TPrA$^+$ cations are crystallographically disordered.

The unit cell of **1** was determined as a function of temperature down to 110 K (data are shown in Figure S10 of the Supporting Information). No phase transition was observed; however, the diffraction peaks broadened as the temperature was lowered. We speculate that this broadening is a result of crystallographic strain resulting from the propyl groups of the cations attempting to attain a more thermodynamically favored conformation. The unit cell lengths and volume decreased monotonically with temperature, with the linear expansion coefficients for the *a* and *c* axes determined to be 8.6 × 10^{-5} K^{-1} and 9.5 × 10^{-6} K^{-1}, respectively, and a volume expansion coefficient of 1.8 × 10^{-4} K^{-1}. Thus, the in-plane expansion is 1 order of magnitude greater than the out-of-plane value.

Compound **2** also adopts a perovskite structure, but rather than crystallizing in a tetragonal 2 × 2 × 2 structure, it forms an orthorhombic $\sqrt{8} \times \sqrt{8} \times 2$ perovskite superlattice as a result of the elongation and contraction of the two *ab* diagonals. Similar to **1**, **2** is characterized by two-dimensional planes formed through single $\mu_{1,5}$-dca$^-$ bridges, which are further linked in the third dimension by single $\mu_{1,5}$-dca$^-$ bridges. The TPrA$^+$ cations reside within the cubic $[Ni(dca)_3]^-$ anion structure. At 298 K, within the *bc* plane, the Ni···Ni separations range from 8.0772(7) to 8.1323(7) Å, whereas along the *a* axis, the metal separations are about 0.5 Å longer, 8.498(1)−8.682(1) Å. When the temperature is lowered to 110 K, the unit cell contracts by 0.32, 0.84, and 0.48% along the three crystallographic axes. Within the *bc* plane, the Ni···Ni separations shorten an average of 0.04(1) Å upon cooling, whereas along the *a* axis, the metal separations shorten by 0.02(1) Å. As expected, at low temperatures, there is less librational disorder in the amide nitrogen atoms of the anion. This is especially noted in the dca anion associated with N19, which is disordered over two sites at room temperature but is ordered at 100 K (see Figure S3a as compared to Figure S4a in the Supporting Information). The TPrA groups are also better defined at 110 K. This is especially evident in the TPrA$^+$ cation associated with N50, which is disordered over two sites at room temperature in a 76:24 ratio, whereas at 110 K, this cation only occupies one orientation (see Figures S3d and S4d in the Supporting Information).

Interestingly, **2** exhibits a re-entrant structural phase transition. At room temperature and at 110 K, this salt belongs to the orthorhombic space group *Pnna*, but between

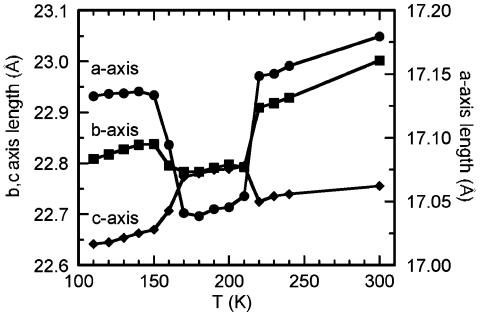

Figure 3. Re-entrant phase transition in **2** as manifested in the unit cell lengths as a function of the temperature. Note that the axes, as labeled, are defined by the orthorhombic cell (the high- and low-temperature phases). The *bc* plane in the orthorhombic space group becomes the *ab* plane in the standard space group setting of the tetragonal space group, where *a* and *b* are reduced by a factor of $1/\sqrt{2}$.

160 and 210 K, a transformation to the tetragonal $P\bar{4}2_1c$ space group occurs, with the *b* and *c* axes becoming identical and a concomitant sharp decrease in the *a* axis (see Figure 3). (The *bc* plane in the orthorhombic structure becomes the *ab* plane in the tetragonal structure in the standard space group settings, and the cell becomes smaller by a factor of $1/\sqrt{2}$ in each of these directions.) In the intermediate phase, a $2 \times 2 \times 2$ perovskite superstructure is, therefore, present, as it is in **1** at all investigated temperatures. At 160 K, the C−N−Ni bond angles range from 164.7(5) to 174.8(8)°; within the *ab* plane, the Ni···Ni separations range from 8.1026(2) to 8.1307(2) Å, whereas along the *c* axis, the metal separations are about 0.4 Å longer, 8.5309(4) Å. The intermediate phase is slightly more isotropic in that the shorter in-plane Ni···Ni separations lengthen and the longer out-of-plane separations contract. The average in-plane separations are 8.10(2), 8.12(2), and 8.05(3) Å, whereas the out-of-plane separations are 8.59(8), 8.5309(4), and 8.57(9) Å at 298, 160, and 110 K, respectively.

Triple Rutile.[21] The (TBA)[M(dca)$_3$] [M = Mn (**3**) and Ni (**4**)] salts crystallize with this motif. A polyhedral representation of this structure is given in Figure 1b. There are four crystallographically independent metal atoms in these structures, each of which lie on a 2-fold axis. As illustrated in Figure 2b, this structure is characterized by doubly bridged (edge-sharing) dimer units, which are further linked by single $\mu_{1,5}$-dca$^-$ bridges to form a three-dimensional anionic network. Thus, each dimer unit is joined to eight adjacent dimers through single $\mu_{1,5}$-dca$^-$ bridges. Hexagonal channels, in which the cations reside, run along the $a + b$ diagonal. In these salts, the octahedral coordination sphere around each of the metal centers consists of the nitrile nitrogen atoms of three crystallographically independent $\mu_{1,5}$-dca$^-$ anions. Each metal atom is joined to four neighboring Mn atoms through single $\mu_{1,5}$-dca$^-$ bridges (corner sharing) and to a fifth through a double $\mu_{1,5}$-dca$^-$ bridge (edge sharing).

For **3**, the Mn−N distances range from 2.200(5) to 2.248(4) Å for the nitrile nitrogen atoms of the single $\mu_{1,5}$-dca$^-$ bridges and from 2.223(4) to 2.243(4) Å for those in the double bridges. The double $\mu_{1,5}$-dca$^-$ bridges occur between Mn1···Mn3 and Mn2···Mn4, with Mn···Mn separations of 7.668(1) and 7.674(1) Å, respectively. The single bridges are about 0.9 Å longer: 8.6302(5) Å (Mn1···Mn2), 8.6288(5) Å (Mn1···Mn4), 8.5473(5) Å (Mn2···Mn3), and 8.5466(5) Å (Mn3···Mn4). The C−N−Mn bond angles range from 150.5(4) to 178.8(5)°.

For **4**, the Ni−N distances range from 2.069(4) to 2.107(5) Å for the nitrile nitrogen atoms of the single $\mu_{1,5}$-dca$^-$ bridges and from 2.064(5) to 2.138(5) Å for the nitrile groups of the double bridges. The double $\mu_{1,5}$-dca$^-$ bridges occur between Ni1···Ni3 and Ni2···Ni4, with Ni···Ni separations of 7.506(1) and 7.508(1) Å, respectively. Similar to the manganese salt, the single $\mu_{1,5}$-dca$^-$ bridges are about 0.9 Å longer: 8.4497(6) Å (Ni1···Ni2), 8.4658(5) Å (Ni1···Ni4), 8.3791(4) Å (Ni2···Ni3), and 8.3942(6) Å (Ni3···Ni4). The C−N−Ni bond angles range from 154.6(5) to 177.1(5)°.

LiSbO$_3$-Type Lattice. The (TPnA)[M(dca)$_3$] [M = Mn (**5**) and Ni (**6**)] salts crystallize in this unique three-dimensional motif, which is characterized by cis bi-bridged zigzag chains, parallel to the *a* axis, which are, in turn, linked by single $\mu_{1,5}$-dca$^-$ bridges (see Figure 2c). Thus, each metal atom is joined to four neighboring *M* atoms through double $\mu_{1,5}$-dca$^-$ bridges (edge sharing) and to two others through a single $\mu_{1,5}$-dca$^-$ bridge (corner sharing). If the difference in bridge type is ignored, the topology of this anionic lattice can be described as a distorted diamondoid net. Polyhedral representations of this structure along two different directions are given in parts c and d of Figure 1. There is one crystallographically independent metal atom in this structure. In these salts, the octahedral coordination sphere around the metal center consists of the nitrile nitrogen atoms of three crystallographically independent nitrile groups. For **5**, the shortest Mn−N$_{nitrile}$ distance occurs for the single $\mu_{1,5}$-dca$^-$ bridges, 2.212(3) Å, with longer Mn−N$_{nitrile}$ bonds, 2.200(3) and 2.252(2) Å, for the double bridges. The C−N−Mn bond angles range from 156.1(2) to 176.6(3)°. The manganese atoms are separated by 7.6964(6) Å along the bi-bridged chains and 8.5144(8) Å through the single $\mu_{1,5}$-dca$^-$ bridges that link the chains. Similarly, for **6**, the shortest Ni−N$_{nitrile}$ distance occurs for the single $\mu_{1,5}$-dca$^-$ bridges, 2.085(2) Å, with slightly longer Ni−N$_{nitrile}$ bonds, 2.094(3) and 2.110(2) Å, for the double bridges. The C−N−Ni bond angles range from 158.7(2) to 175.0(2)°. The nickel atoms are separated by 7.5343(4) Å along the bi-bridged chains and 8.3832(6) Å through single $\mu_{1,5}$-dca$^-$ bridges that link the chains.

Magnetism. Direct Current Susceptibility. Each of the Mn salts possesses a room temperature χT value of approximately 4.1 emu K/mol, (see Table 2), which is in good agreement with the value expected for isolated $S = {}^5/_2$ ions, that is, 4.375 emu K/mol. For all six compounds, the reciprocal magnetic susceptibility, $1/\chi$, was fitted to the Curie−Weiss expression, $\chi = Ng^2\mu_B{}^2S(S + 1)/3k_B(T - \theta)$, over the full temperature range, the results of which are presented in Table 2. The small (and negative) θ values suggest very weak antiferromagnetic interaction between the spin carriers or zero-field splitting, the latter generally being

(21) A simple rutile contains infinite doubly bridged chains. The triple rutile, with its dimers, is formed by systematically removing every third metal center along the chain.

Table 2. Summary of Magnetic Data Obtained from Theoretical Fits to $\chi T(T)$ for Compounds **1**−**6**, as Described in the Text

compound	χT (emu K/mol)[a]	g value[b]	θ (K)[b]	g value[c]	J/k_B (K)	$\lvert D\rvert/k_B$ (K)
1	4.096	1.954(1)	−2.4(2)	1.951(2)	−0.060(1)	
2	1.278	2.261(3)	−4.7(4)	2.266(2)		3.02(3)
3	4.08	1.950(1)	−2.0(2)	1.949(2)	−0.059(1)	
4	1.211	2.201(2)	−2.9(3)	2.196(2)		3.20(3)
5	4.125	1.942(1)	−2.0(2)	1.942(2)	−0.39(1)[d]	
6	1.144	2.138(2)	−4.4(3)	2.128(2)		1.98(1)

[a] At 300 K. [b] From Curie−Weiss fit. [c] Parameters determined from fits to a three-dimensional Rushbrooke−Wood antiferromagnetic model[22] (**1** and **3**), one-dimensional Fisher chain model[23] (**5**), and zero-field splitting model of (**2**, **4**, and **6**). [d] Residual interchain interactions were obtained by a mean-field correction that yielded $zJ'/k_B = -0.075(1)$ K.

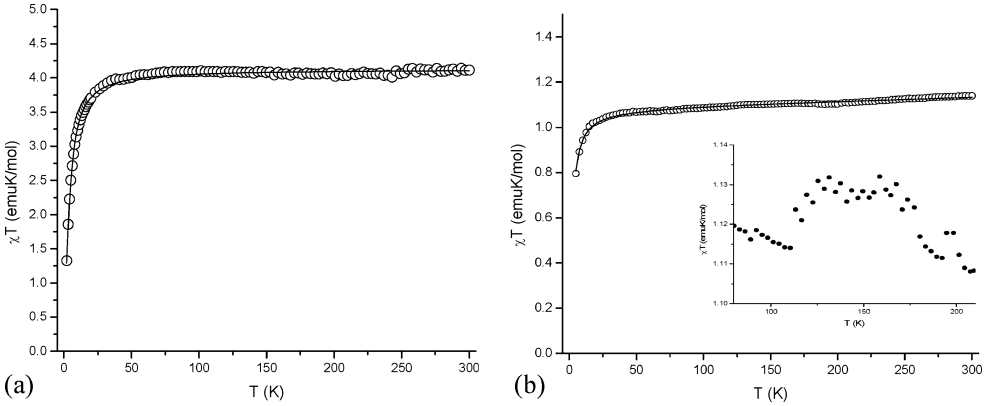

Figure 4. (a) Fit to the χT vs T data for **5**. (b) Fit to the χT vs T data for **6**; inset shows the re-entrant phase transition for **2** and its effect on χT.

negligible for high-spin Mn^{2+} ions. Because the Mn···Mn distances are similar for compounds **1** and **3**, the magnetic data can be modeled by an exchange Hamiltonian, $\mathscr{H} = -J\sum S_iS_{i+1}$, based on a $S = {}^5/_2$ three-dimensional simple cubic antiferromagnetic model.[22] A polynomial approximation to the susceptibility based on this model is given by eq 1, where $x = J/k_BT$, $c_1 = 35$, $c_2 = 221.67$, $c_3 = 608.22$, $c_4 = 26049.66$, $c_5 = 210986$, and $c_6 = 8014980$. Least-squares fits of the data gave $g = 1.951(2)$ and $J/k_B = -0.060(1)$ K (**1**) and $g = 1.949(2)$ and $J/k_B = -0.059(1)$ K (**3**).

$$\chi_{3D} = \frac{35Ng^2\mu_B{}^2}{12k_BT}(1 + c_1x + c_2x^2 + c_3x^3 + c_4x^4 + c_5x^5 + c_6x^6) \quad (1)$$

The metal−metal separations in **5** indicate a nearly 1 Å difference in the Mn···Mn distances, and thus, the data were fit to a Fisher one-dimensional chain model (eq 2),[23] with

$$\chi_{1D} = \frac{Ng^2\mu_B{}^2S(S+1)}{3k_BT}\frac{1+u(K)}{1-u(K)}, \qquad u(K) = \frac{2JS(S+1)}{k_BT} - \frac{k_BT}{2JS(S+1)} \quad (2)$$

the addition of a mean-field term[24] to account for residual intermolecular interactions between the bi-bridged chains. As shown in Figure 4a, the result of this fit yielded good agreement for $g = 1.943(1)$, $J/k_B = -0.39(1)$ K, and $zJ'/k_B = 0.075(1)$ K. The resulting small J values signify a weak exchange interaction mediated by the μ-bonded dca linkages in these structures.

In the case of the Ni^{2+} compounds, a more likely scenario for the deviations from a simple Curie model is a zero-field splitting of the ${}^3A_{2g}$ ground state and an exchange Hamiltonian of $\mathscr{H} = -J\sum S_iS_{i+1} + D\sum(S_i^z)^2 + g\mu_\beta B\sum S_i$.[25] Thus, the χT data for the three Ni salts were fitted to eq 3, where $x = |D|/k_BT$ and $|D|/k_B$ values of 3.02(3), 3.20(3), and 1.98(1) K were obtained for compounds **2**, **4**, and **6**, respectively (see Figure 4b). We give the absolute values here because the sign of D can only be determined by measurements on single crystals. The fitted g values for the Ni salts deviate appreciably from the free electron value and reflect the single-ion anisotropy typically associated with this ion. The decreasing slope of χT is due to a temperature-independent paramagnetism of the Ni^{2+} ion. Finally, as illustrated in the inset of Figure 4b, the anomalies observed in each of the lattice parameters for **2** do affect the χT data, which shows anomalous behavior in the same region.

$$\chi_{ZFS} = \frac{Ng^2\mu_B{}^2}{k_BT}\left(\frac{2e^{-x} + \frac{4}{x}(1+e^{-x})}{1+2e^{-x}}\right) \quad (3)$$

Alternating Current Susceptibility. As shown in Figure 5a, the ac susceptibility of a large (19.064 mg) single crystal of the **1** salt was measured, in the absence of an external magnetic field, along each of the principal crystallographic axes. The orientational dependence of $\chi'(T)$ clearly indicates the onset of three-dimensional antiferromagnetic ordering below 2.1 K. The parallel susceptibility, $\chi_{||}$, reaches a

(22) Rushbrooke, G. S.; Wood, P. J. *Mol. Phys.* **1958**, *1*, 257.
(23) Fisher, M. E. *Am. J. Phys.* **1964**, *32*, 343.
(24) Carlin, R. L. *Magnetochemistry*; Springer-Verlag: New York, 1986.
(25) Kahn, O. *Molecular Magnetism*; VCH Publishers: New York, 1993.

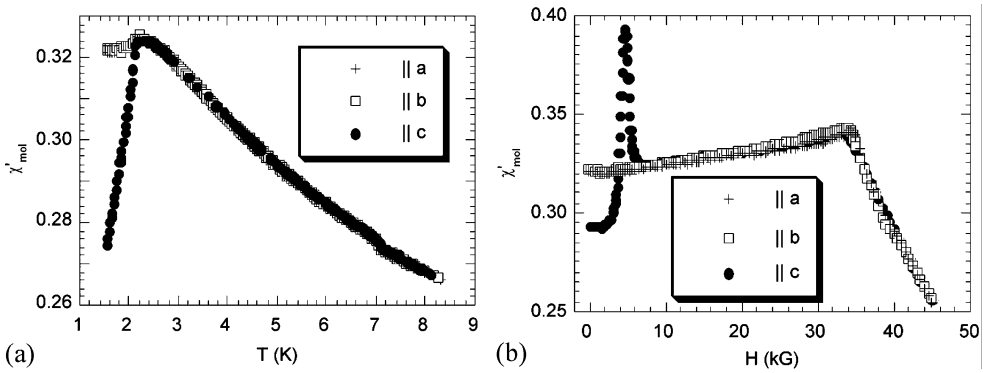

Figure 5. Alternating current susceptibility data for a single crystal of **1** measured along the three crystallographic axes. (a) Temperature dependence. (b) Field dependence.

maximum just above T_N and decreases rapidly upon cooling further to 1.6 K, as expected for this orientation. Two perpendicular components of the susceptibility, that is, $\chi_\perp$, are observed where each reaches a subtle maximum near T_N and remain essentially invariant below this. The point at which $\chi_{||}$ and $\chi_\perp$ diverge is defined as T_N. Similar behavior was observed for a single crystal of **3**, which yielded a slightly lower T_N of 1.8. Only a polycrystalline sample of **5** was available, which displayed a broad maximum near 2.2 K, similar in shape to polycrystalline measurements on **1** and **3**.

Isothermal ac magnetic susceptibility measurements as a function of a dc magnetic field were performed at 1.8 K. As shown in Figure 5b, when H was applied parallel to the c axis, a sharp peak was observed at 0.46 T for **1**, suggesting the onset of a spin-flop transition, H_{sf}.[26] This peak was less pronounced in samples of **3** and **5**. Analogous measurements along the a and b axes yielded no such peak at 0.46 T, which indicates that c is the magnetic easy axis. Above H_{sf}, d$M(H)$/dH increases linearly to 3.35 T, at which point a transition to the paramagnetic phase, H_c, occurs, as indicated by a rapid decrease in d$M(H)$/dH for all three crystal orientations. Similar field-dependent behavior has been observed in Mn(dca)$_2$(pyz), which has $T_N = 2.53$ K, $H_{sf} = 0.43$ T, and $H_c = 2.83$ T.[27] Likewise, the values of H_{sf} and H_c can be used to estimate the exchange (H_E) and anisotropy (H_A) fields.[28] From the mean-field results given in eqs 4 and 5,[26] we obtain 1.643 and 0.064 T for H_E and H_A, respectively. Not surprisingly, these values are also comparable to those found for Mn(dca)$_2$(pyz).[27]

$$H_{sf} = \sqrt{2H_E - {H_A}^2} \quad (4)$$

$$H_c = 2H_E - H_A \quad (5)$$

Similar ac susceptibility measurements of polycrystalline samples of the nickel salts (**2**, **4**, and **6**) found exponentially decreasing susceptibility with increasing temperature and no indication of a maximum, which would be indicative of long-range magnetic order.

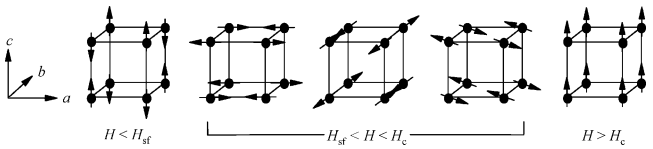

Figure 6. Illustration of the proposed magnetic structures for **1** at low, intermediate, and high fields.

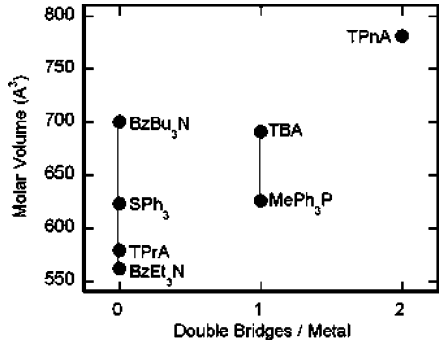

Figure 7. Plot of the molar volume of the (TAA)[Mn(dca)$_3$] salts as a function of the number of double dca bridges per metal center. Structures with no double bridges per metal center form perovskite-type frameworks, those with one double dca bridge per metal center form triple rutile structures, and the (TPnA)[Mn(dca)$_3$] structure, with two double dca bridges per metal center, forms a $LiSbO_3$-type structure.

Proposed Magnetic Structures for 1. Knowing that the easy axis of magnetization lies along the c direction, we can propose spin configurations for $T < T_N$ in each of the three distinct regions of the phase diagram, that is, $H < H_{sf}$, $H_{sf} < H < H_c$, and $H > H_c$. As illustrated in Figure 6, the ground-state magnetic structure of **1** consists of a collinear arrangement of antiferromagnetically coupled Mn^{2+} moments parallel to c. The application of a magnetic field equivalent to H_{sf} forces the moments to "flop" perpendicular to H. In this phase, however, there are three possible spin configurations that could occur owing to the tetragonal symmetry of the structure. The spins will likely be confined to the ab plane but could orient themselves along either a, b, or the ab diagonal, depending on subtle differences in anisotropy. For the high-field phase, that is, above H_c, the spins will align parallel to H but in a ferromagnetic-like arrangement. It should be noted that, except for H_{sf} and H_c, the moments continually rotate with the applied magnetic field.

(26) de Jongh, L. J.; Miedema, A. R. *Adv. Phys.* **2001**, *50*, 947.
(27) Manson, J. L.; Huang, Q. Z.; Lynn, J. W.; Koo, H. J.; Whangbo, M. H.; Bateman, R.; Otsuka, T.; Wada, N.; Argyriou, D. N.; Miller, J. S. *J. Am. Chem. Soc.* **2001**, *123*, 162.
(28) Eqs 4 and 5 are the mean-field results obtained at $T = 0$. However, we can extrapolate them to 1.8 K and approximate H_E and H_A.

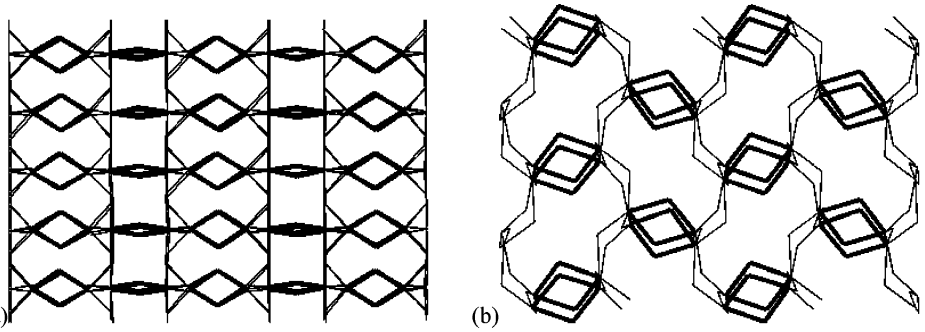

Figure 8. Stick diagram, as projected on the *ac* plane, illustrating the differences between the anionic networks found in (a) TBA[*M*(dca)$_3$] (*M* = Mn and Ni) and (b) (MePh$_3$P)[Mn(dca)$_3$].[9] In both illustrations, the *c* axis lies horizontal, whereas the *a* axis is vertical. The dca ligands that form double bridges are illustrated as thick lines, whereas those associated with single bridges are shown as thin lines.

Infrared Spectroscopy. The cyano stretching region of the infrared spectra for the (TAA)[Mn(dca)$_3$] complexes are all quite similar to the vibrational frequencies, averaging 2290 ± 3 cm^{-1}, 2237 ± 2 cm^{-1}, and 2170 ± 5 cm^{-1}. These absorption bands have previously been assigned as the ν_{as+s}, ν_{as}, and ν_s modes, respectively.[29,30] Compared to the binary *M*(dca)$_2$ complexes, the ν_{as} and ν_s modes in the (TAA)[*M*(dca)$_3$] salts are shifted to lower wavenumbers (see Figure S11 in the Supporting Information). This is understood by the fact that the dca ligands in the (TAA)[*M*(dca)$_3$] salts possess a higher charge density than in the neutral *M*(dca)$_2$ complexes.[11] The ν_{as+s} mode is the same for both the nickel (2291 ± 2 cm^{-1}) and manganese complexes. The ν_{as} mode is slightly higher in energy for the **3** and **5** derivatives (2242 ± 2 cm^{-1}) and notably higher for the **1** (2254 ± 2 cm^{-1}) salt as compared to the manganese analogues. Similarly, the ν_s mode is slightly higher in energy for the nickel derivatives **3** and **5** (2181 ± 2 cm^{-1}) and notably higher for **1** (2190 ± 2 cm^{-1}). These infrared modes, which have frequently been used to identify the coordination number of the dca ligand,[31] are consistent with bidendate coordination.

Discussion

The [*M*(dca)$_3$]$^-$ anion can conform to the templates of various cations, thus, forming various structure types. Although the anionic structure is generally templated by the cation, the metal coordination also affects the topology. The anion structures of the (Bz*R*$_3$N)[*M*(dca)$_3$] (*R* = Bu and Et; *M* = Mn, Fe, and Co)[13] and (TPrA)[*M*(dca)$_3$] salts are related in that both contain a three-dimensional network of single $\mu_{1,5}$-dca$^-$ bridges, forming a perovskite (simple cubelike, α-polonium, or ReO$_3$) structure. The anion in the (Bz*R*$_3$)[*M*(dca)$_3$] salts form simple parallelepipeds, but the cubelike structure in the TPrA$^+$ salts is more complex, with none of the *M*−*M*−*M* angles being 90°. The C−N−Mn bond angles in (BzBu$_3$N)[Mn(dca)$_3$] are essentially linear (>175.1°), whereas for the related salt with a smaller cation, (BzEt$_3$N)[Mn(dca)$_3$], these angles are more acute (>169.91°). For the compounds discussed in this paper, some C−N−*M* bond angles are considerably more acute, with some less than 160°. The adjacent Mn···Mn separations in (BzBu$_3$N)[Mn(dca)$_3$] are 8.825−8.909 Å, considerably longer than those in (BzEt$_3$)[Mn(dca)$_3$] (8.176−8.302 Å). (TPrA)[Mn(dca)$_3$] has short Mn···Mn separations, ∼8.25 Å, within the *ab* plane, with ∼0.5 Å longer Mn···Mn distances in the third dimension. As illustrated in Figure 7, the molar volume of these (TAA)[Mn(dca)$_3$] salts range from 562 Å^3 for (BzEt$_3$N)[Mn(dca)$_3$] to 700 Å^3 for (BzBu$_3$N)[Mn(dca)$_3$], with (TPrA)[Mn(dca)$_3$] having an intermediate value of 579 Å^3.

When the larger TBA$^+$ cation is used as a template, a triple rutile-type structure forms with one double dca bridge per metal center. The TBA$^+$ salt has a larger molar volume (692 Å^3) than that observed in the related TPrA$^+$ salt. Similar to the (MePh$_3$P)[Mn(dca)$_3$] salt,[9] the metals in the TBA$^+$ salts (**3** and **4**) are five-connecting centers, by which each end of a bi-bridged dimer is linked through single dca bridges to four other dimerized units. However, as illustrated in Figure 8, the topologies in these anionic lattices are different. The bi-bridged units in the TBA$^+$ salts are arranged linearly and alternately twist 90° along the *c* axis. In contrast, the dimerized units are staggered along the *c* axis in the (MePh$_3$P)[Mn(dca)$_3$] structure, but the dimers are nearly coplanar with each other. The dimer-like Mn···Mn distances in (MePh$_3$P)[Mn(dca)$_3$] are slightly shorter (7.52 Å) than those in (TBA)[Mn(dca)$_3$] (7.67 Å). In the (MePh$_3$P)[Mn(dca)$_3$] structure, the single $\mu_{1,5}$-dca- bridges can be identified as "in-plane" (7.828 and 7.941 Å) or "out-of-plane" (8.685 and 8.702 Å), whereas these single $\mu_{1,5}$-dca- bridges are more uniform (8.547 to 8.630 Å) in the (TBA)[Mn(dca)$_3$] structure.

When the larger TPnA$^+$ cation is used as the template, a novel LiSbO$_3$ structure type (cis bi-bridged zigzag chains) forms that has not previously been identified among [*M*(dca)$_3$]$^-$ salts. This structural type has two dca$^-$ bridges per metal center. This structural motif is apparently necessitated by the requirements of the larger cation, leading to a less dense anionic structure with a molar volume of 781 Å^3.

This relationship between the molar volume and the number of double dca$^-$ bridges in the (TAA)[Mn(dca)$_3$] structures presents a paradox: one might think that the less-dense structures would be constructed of single dca$^-$ bridges because they are typically about 1 Å longer than double dca$^-$ bridges. However, the transformation to a less-dense anionic

(29) Köhler, V. H.; Kolbe, A.; Lux, G. *Z. Anorg. Allg. Chem.* **1977**, *428*, 103.
(30) Manson, J. L.; Kmety, C. R.; Epstein, A. J.; Miller, J. S. *Inorg. Chem.* **1999**, *38*, 2552.
(31) Golub, A. M.; Kohler, H.; Skopendo, V. V. In *Chemistry of Pseudohalides*; Clark, R. J. H., Ed.; Elsevier: Amsterdam, 1986; Vol. 21.

structural motif is achieved for the larger cations through a reconstruction of the anion lattice.

Conclusions

A series of three-dimensional anionic $[M(dca)_3]^-$ (M = Mn and Ni) has been prepared through the use of three TAA^+ cationic templates. The identity of the cation dictates the structural type of the anion. The $TPrA^+$ salts crystallize in a perovskite-type structure with single $\mu_{1,5}$-dca^- bridges connecting the octahedral metal centers to form an α-polonium cubic-type anion structure. The TBA^+ salts yield rutile-type structures in which single $\mu_{1,5}$-dca^- bridges link together dimer-like (bi-bridged) metal centers. The $TPnA^+$ salts crystallize in a $LiSbO_3$-type structure in which doubly bridged chains are linked into a three-dimensional structure through single $\mu_{1,5}$-dca^- linkages. The molar volume of the three-dimensional anionic $[Mn(dca)_3]^-$ framework increases from 579 to 781 Å^3 as the size of the templating cation increases from $TPrA^+$ to $TPnA^+$. The manganese salts exhibit long-range antiferromagnetic ordering below 2.1 K, whereas no long-range magnetic order was observed in the nickel analogues. This can be rationalized by the fact that, in an isostructural series of salts, T_N typically scales with the value of S (the number of unpaired electrons). The nickel salts may also magnetically order, but at a much lower temperature.

Acknowledgment. Work at Argonne National Laboratory was supported by the Office of Basic Energy Sciences, Division of Materials Science, U.S. Department of Energy, under Contract W-31-109-ENG-38.

Supporting Information Available: X-ray crystallographic details, including selected bond lengths and angles, in CIF format, thermal ellipsoid plots with atom labeling for compounds **1**−**6**, a plot of the unit cell parameters for **1** as a function of temperature, and infrared spectroscopy data. This material is available free of charge via the Internet at http://pubs.acs.org.

IC0484598